Remote Sensing of Environment 135 (2013) 189–201

Contents lists available at SciVerse ScienceDirect

Remote Sensing of Environment

journal homepage: www.elsevier.com/locate/rse

Phenology and gross primary production of two dominant savanna woodland ecosystems in Southern Africa

Cui Jin [a], Xiangming Xiao [a,*], Lutz Merbold [b], Almut Arneth [c], Elmar Veenendaal [d], Werner L. Kutsch [e]

[a] Department of Microbiology and Plant Biology, Center for Spatial Analysis, University of Oklahoma, Norman, OK 73019, USA
[b] Department of Environmental Systems Science, Institute for Agricultural Sciences (IAS), Grassland Sciences Group, ETH Zurich, 8092 Zurich, Switzerland
[c] Karlsruhe Institute of Technology, Institute of Meteorology and Climate research/Atmospheric Environmental Research, Kreuzeckbahn Str., 19, 82467 Garmisch–Partenkirchen, Germany
[d] Nature Conservation and Plant Ecology Group, Wageningen University, Droevendaalsesteeg 3a, 6700 PB Wageningen, The Netherlands
[e] Institute for Climate-Smart Agriculture, Thünen-Institute, Bundesallee 50, 38116, Braunschweig, Germany

ARTICLE INFO

Article history:
Received 8 October 2012
Received in revised form 21 March 2013
Accepted 26 March 2013
Available online xxxx

Keywords:
Vegetation Photosynthesis Model (VPM)
LSWI
Eddy covariance
Vegetation indices
MODIS

ABSTRACT

Accurate estimation of gross primary production (GPP) of savanna woodlands is needed for evaluating the terrestrial carbon cycle at various spatial and temporal scales. The eddy covariance (EC) technique provides continuous measurements of net CO_2 exchange (NEE) between terrestrial ecosystems and the atmosphere. Only a few flux tower sites were run in Africa and very limited observational data of savanna woodlands in Africa are available. Although several publications have reported on the seasonal dynamics and interannual variation of GPP of savanna vegetation through partitioning the measured NEE data, current knowledge about GPP and phenology of savanna ecosystems is still limited. This study focused on two savanna woodland flux tower sites in Botswana and Zambia, representing two dominant savanna woodlands (mopane and miombo) and climate patterns (semi-arid and semi-humid) in Southern Africa. Phenology of these savanna woodlands was delineated from three vegetation indices derived from Moderate Resolution Imaging Spectroradiometer (MODIS) and GPP estimated from eddy covariance measurements at flux tower sites (GPP_{EC}). The Vegetation Photosynthesis Model (VPM), which is driven by satellite images and meteorological data, was also evaluated, and the results showed that the VPM-based GPP estimates (GPP_{VPM}) were able to track the seasonal dynamics of GPP_{EC}. The total GPP_{VPM} and GPP_{EC} within the plant growing season defined by a water-related vegetation index differed within the range of ±6%. This study suggests that the VPM is a valuable tool for estimating GPP of semi-arid and semi-humid savanna woodland ecosystems in Southern Africa.

1. Introduction

Savannas are one of the most widely distributed vegetation types, covering one-fifth of the earth land surface (Scholes & Hall, 1996). A recent modeling study estimated an annual sum of about 30 Pg C gross primary production (GPP) from tropical savannas and grasslands, accounting for 25.7% of the global terrestrial GPP (Beer et al., 2010). Africa, which is dominated by the largest area of savanna ecosystems in the world, is considered a main source of uncertainty in the global terrestrial carbon cycles (Weber et al., 2009; Williams et al., 2007). Current knowledge of Africa's carbon fluxes and storage is still limited due to the spatial extent, fire disturbance, and high interannual variability in climate and productivity (Ciais et al., 2011; Williams et al., 2007; Woollen et al., 2012).

Mopane and miombo woodlands in South and Central Africa covering 3.6 million km^2 of land are the single largest dry woodlands in the world. Over the past decade, continuous fluxes of carbon, water, and energy between the land surface and the atmosphere, as measured with the eddy covariance technique, have been used to study the temporal dynamics and spatial pattern of the carbon cycle of savanna woodlands in Southern Africa (Archibald et al., 2009; Kutsch et al., 2008; Merbold et al., 2009, 2011; Scanlon & Albertson, 2004; Veenendaal et al., 2004; Williams et al., 2009). However, such measurements have been made at only a few sites and often over short time periods (Veenendaal et al., 2004).

Satellite remote sensing at moderate spatial resolutions provides daily observations of land surface properties at the spatial scale compatible with the footprint sizes of the eddy covariance observation sites. It has become a more and more important data source for the study of vegetation phenology (Alcantara et al., 2012; Brown et al., 2012; Jones et al., 2012; Kim et al., 2012; Kross et al., 2011; White et al., 2009) and GPP estimates (Gitelson et al., 2012; Kalfas et al., 2011; Peng et al., 2011; Sakamoto et al., 2011; Sjöström et al., 2009; Wang et al., 2010b; Wu, 2012; Wu & Chen, 2012; Zhang et al., 2012).

* Corresponding author at: Department of Microbiology and Plant Biology, University of Oklahoma, 101 David L. Boren Blvd., Norman, OK 73019, USA. Tel.: +1 405 325 8941.
E-mail address: xiangming.xiao@ou.edu (X. Xiao).

0034-4257/$ – see front matter © 2013 Elsevier Inc. All rights reserved.
http://dx.doi.org/10.1016/j.rse.2013.03.033

Vegetation phenology is a fundamental determinant affecting the ecosystem processes of carbon, water, and energy exchange (Larcher, 2003). It determines the timing and duration of a photosynthetically active canopy and influences the magnitude of carbon and water fluxes throughout the plant growing season (Jolly & Running, 2004). The vegetation indices calculated from the reflectance of spectral bands have been proved to effectively monitor the vegetation phenology (Bradley et al., 2007; Moody & Johnson, 2001; Sakamoto et al., 2005; Xiao, 2006; Zhang et al., 2006). Earlier studies of phenology have focused on vegetation indices derived from visible and near infrared bands, for example, the Normalized Difference Vegetation Index (NDVI), which is calculated as a normalized ratio between near infrared and red spectral bands (Tucker, 1979), and the Enhanced Vegetation Index (EVI), which is calculated from blue, red, and near infrared bands (Huete et al., 2002). Both NDVI and EVI have been shown to effectively track the seasonality and spatial patterns of savanna phenology (Archibald & Scholes, 2007; Chidumayo, 2001; Higgins et al., 2011; Huttich et al., 2011). It is well known that the shortwave infrared band (SWIR) is sensitive to water in vegetation and soil. One SWIR-based vegetation index is the Land Surface Water Index (LSWI), which is calculated from near infrared (NIR) and SWIR (Xiao et al., 2004a, 2004b). It has been successfully applied to vegetation phenology study and phenology-based land cover mapping (Cai et al., 2011; Chandrasekar et al., 2010; Park & Miura, 2011; Xiao et al., 2004a, 2006). A prior study has already indicated that LSWI was sensitive to the wet and dry conditions in Africa (Tian et al., 2012). Therefore, whether the time-series LSWI data can effectively extract the phenological dynamics of savanna woodlands in Southern Africa across precipitation gradient and woodland species types is the first question addressed in this study. Water availability at the regional scale, an important seasonal driver for savanna vegetation growth, is the primary limit for predicting savanna phenology patterns (Archibald & Scholes, 2007).

A number of the satellite-based Production Efficiency Models (PEMs) have been developed to estimate GPP of vegetation as the product of the absorbed photosynthetically active radiation (APAR) and the light use efficiency (Coops, 1999; Monteith, 1972; Potter et al., 1993; Prince et al., 1995; Ruimy et al., 1996). In one group of PEMs, the greenness-related vegetation indices are used to estimate APAR by the canopy. NDVI is most commonly used in the earlier PEMs (Potter et al., 1993; Prince & Goward, 1995; Ruimy et al., 1994; Running et al., 2000; Veroustraete et al., 2004; Yuan et al., 2007). In the other group of PEMs, chlorophyll-related vegetation indices such as EVI and chlorophyll index are used to estimate APAR by chlorophyll (Gitelson et al., 2006; Potter et al., 2012; Sims et al., 2006; Xiao et al., 2004a, 2004b).

The Vegetation Photosynthesis Model (VPM) is the satellite-based PEMs that used the concept of chlorophyll and light absorption by chlorophyll (Xiao et al., 2004a, 2004b). The VPM has been extensively verified for temperate, boreal and moist tropical evergreen forests (Xiao et al., 2004a, 2004b, 2005a, 2005b, 2006), temperate and plateau grassland (Li et al., 2007; Wu et al., 2008) as well as agricultural ecosystems (Kalfas et al., 2011; Wang et al., 2010b). However, its performance in simulating GPP of savanna woodland ecosystems is still unknown.

The objectives of this study are twofold: (1) to evaluate the potential of remote sensing vegetation indices (NDVI, EVI, and LSWI) in identifying land surface phenology of savanna woodlands and determining the growing season length; and (2) to examine the potential of the VPM to simulate GPP of two dominant savanna woodland sites differing in annual precipitation and vegetation composition in Southern Africa. The leaf-on and leaf-off phenological phases need to be identified and then used to evaluate the performance of satellite-based PEMs that estimate GPP of savanna woodland ecosystems. Although a vast area in Southern Africa is covered with mopane and miombo woodlands, there are only two sites with continuous measurements of CO_2 net exchange between the woodlands and the atmosphere by eddy covariance technique; and in this study we used data from the two sites, located in Botswana and Zambia.

2. Materials and methods

2.1. Study sites

These two eddy covariance flux sites of savanna woodlands are within the Kalahari Transect (KT) in Southern Africa, one of the International Geosphere–Biosphere Program (IGBP) Transects for quantifying biogeochemistry and primary production, water and energy balance, ecosystem structure and function at the continental scale (Scholes & Parsons, 1997). Both sites are located along a precipitation gradient in the semi-arid and sub-humid regions of Southern Africa. The geo-locations and landscape features of these two sites are shown in Fig. 1 and Table 1. Detailed descriptions of the two sites can be obtained via FLUXNET — a global network of micrometeorological tower sites (http://www.fluxnet.ornl.gov/fluxnet/sitesearch.cfm) and site specific publications (Arneth et al., 2006; Merbold et al., 2011; Veenendaal et al., 2004, 2008).

The Botswana site (Maun, 19.9165°S, 23.5603°E) is dominated by broadleaf deciduous woodland (*Colophospermum mopane*) with a sparse understory of grasses, a typical mopane woodland. The climate is characterized as semi-arid, with a distinct dry season (May–September) and wet season (December–March) and a mean annual precipitation (MAP) of 464 mm (Veenendaal et al., 2004, 2008). The vegetation is relatively homogenous over a large area around the site (at 2.5 km in all directions) (Fig. 1). Maximum leaf area index (LAI) is around 1.0 during the wet season (Tian et al., 2002). For decades, this area was disturbed by various human activities, e.g. cattle grazing. This disturbance has been largely eliminated since the site was set up.

The Zambian site is situated at the Kataba Forest Reserve, 20 km south of Mongu in Western Zambia (Mongu, 15.4388°S, 23.2525°E). The site has a semi-humid climate with distinct wet and dry seasons. The mean annual precipitation is 945 mm, occurring from mid-October to April of the following year. The maximum monthly temperature ranges from 23 °C to 32 °C. The vegetation is broadleaf deciduous miombo woodland, dominated by *Brachystegia spiciformis* (24.7%), *bakerana* (29.8%), *Guibourtia coleosperma* (16.8%), and *Ochna pulchra* (24.5%). The canopy cover is about 70%, and LAI has strong seasonal dynamics ranging from 0.8 to 1.68. The ground-based fraction of absorbed photosynthetically active radiation (FPAR) was measured once a month during 2000–2002, and showed strong seasonal dynamics with the range of 0.2 in September to 0.6 in January (Huemmrich et al., 2005). Some land use activities were permitted in this area, including livestock grazing and firewood collection. Low intensity ground fires happened frequently. However, serious land cover changes caused by intense charcoal production and the conversion from woodlands to agricultural land happened in the surrounding areas during recent years (Kutsch et al., 2011; Merbold et al., 2011).

2.2. Site-specific meteorological data and CO_2 flux data

All meteorological and CO_2 flux data used in this study were downloaded from CarboAfrica data portal (http://gaia.agraria.unitus.it/newtcdc2/CarboAfrica_home.aspx). It provides the meteorological and CO_2 flux datasets at half hourly, daily, 8-day, and monthly intervals. Meteorological data and CO_2 fluxes of the two sites were available for the periods of 1999–2001 and 2007–2009 (Figs. 2 and 3). The precipitation data in 2008/2009 at the Mongu site was incomplete due to a sensor malfunction. We used precipitation data from the Zambian Meteorological Department (20 km away) to replace the missing data. At the Maun site, precipitation started in late-November and lasted until May of the next year. Annual rainfall was 197 mm in 2000/2001 and 431 mm in 1999/2000, respectively. The wet season at the Mongu site was concentrated from mid-October to the end of

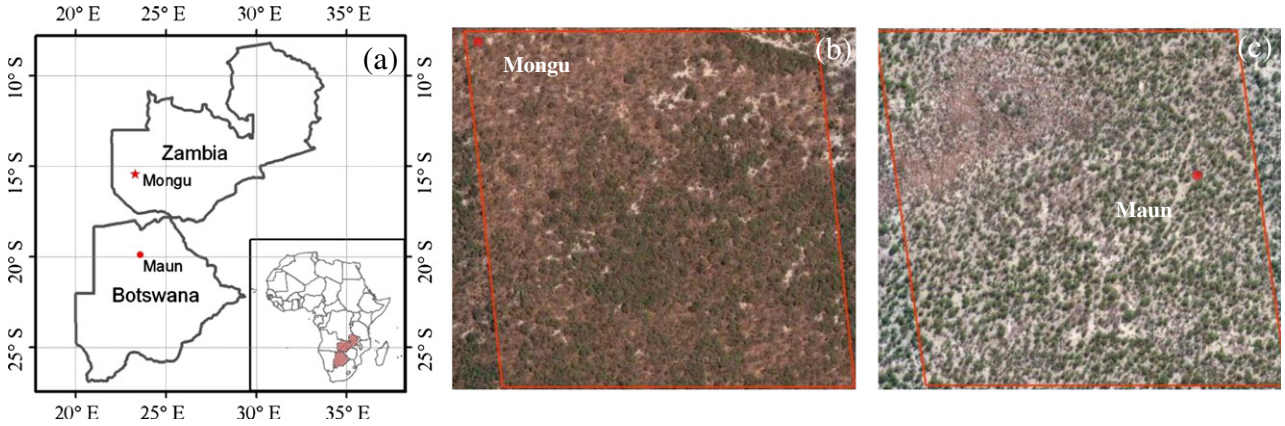

Fig. 1. A simple illustration of the study sites, including (a) geo-locations of two savanna woodland flux tower sites in Southern Africa; (b) landscapes at the Mongu site, Zambia, background image — Google Earth on 09/18/2005; (c) landscapes at the Maun site, Botswana, background image — Google Earth on 07/06/2011. The red square line in (b) and (c) corresponds to the size of one MODIS pixel at 500-m spatial resolution, and the red dots represent the locations of the flux towers. The website http://eomf.ou.edu/visualization/gmap/ provides visualization of flux tower site location and MODIS pixel boundary. (For interpretation of the references to color in this figure legend, the reader is referred to the web version of this article.)

March of the next year, and annual precipitation was 1160 mm in 2007/2008 and 1205 mm in 2008/2009 (Fig. 2).

The 8-day Level 4 datasets contain air temperature, precipitation, PAR, GPP, and NEE. NEE is gap-filled by two mathematical algorithms: the Marginal Distribution Sampling (MDS) (Reichstein et al., 2005) and the Artificial Neural Network (ANN) approach as described in Papale and Valentini (2003). In this study, we used the standardized GPP dataset partitioned from NEE generated with the MDS approach. We carefully evaluated the NEE and GPP data, and identified questionable observations (Fig. 3). At the Maun site, three 8-day periods during December 2000 and January 2001 showed extremely large variations of NEE and GPP (in the range of 40% to 100% in comparison with its neighboring 8-day periods), we treated them as outliers and excluded them in data analysis (Fig. 3a).

2.3. MODIS land surface reflectance, vegetation indices, and GPP products

The Moderate Resolution Imaging Spectroradiometer (MODIS) onboard the Terra and Aqua satellites provide global coverage of imagery every one to two days from 36 spectral bands. This study used the MODIS Land Surface Reflectance 8-Day L3 Global 500 m products (MOD09A1, Collection 5). MOD09A1 provides land surface reflectance from seven spectral bands: red (620–670 nm), NIR_1 (841–876 nm), blue (459–479 nm), green (545–565 nm), NIR_2 (1230–1250 nm), $SWIR_1$ (1628–1652 nm), and $SWIR_2$ (2105–2155 nm). There are forty-six MOD09A1 8-day composites within a year. The time-series MOD09A1data (2/2000 to 12/2011) for the Maun and Mongu sites were extracted from the MODIS data portal at the Earth Observation and Modeling Facility (EOMF), University of Oklahoma (http://www.eomf.ou.edu/visualization/manual/).

For each MODIS 8-day observation of surface reflectance, three vegetation indices were calculated using surface reflectance (ρ) from the blue, red, NIR_1, and $SWIR_1$ bands: (1) NDVI (Tucker, 1979), (2) EVI (Huete et al., 1997, 2002), and (3) LSWI (Xiao et al., 2004b, 2005b).

$$NDVI = \frac{\rho_{NIR_1} - \rho_{red}}{\rho_{NIR_1} + \rho_{red}} \quad (1)$$

$$EVI = \frac{\rho_{NIR_1} - \rho_{red}}{\rho_{NIR_1} + 6 \times \rho_{red} - 7.5 \times \rho_{blue} + 1} \quad (2)$$

$$LSWI = \frac{\rho_{NIR_1} - \rho_{SWIR_1}}{\rho_{NIR_1} + \rho_{SWIR_1}}. \quad (3)$$

The vegetation indices calculated from surface reflectance contained noise caused by cloud, cloud shadow, atmospheric aerosols, and the large observing angle. The quality flags of MOD09A1 files showed many bad-quality observations over the course of the wet season for the Mongu site. If the quality flag of an observation listed cloud, cloud shadow, aerosol quality, or adjacency to cloud, the observation was marked as unreliable. Built upon the two-step gap-filling procedure reported in earlier studies (Xiao et al., 2004b), we used a three-step gap-filling procedure to gap-fill vegetation index time series data. Step 1 deals with only one bad-quality observation (x(t)). We defined a filter with a three-observation moving window (x(t − 1), x(t) and x(t + 1)) and used data considered to be of good quality or reliable observations to correct or gap-fill unreliable observations. If both x(t − 1) and x(t + 1) pixels were reliable and x(t) was unreliable, the average of x(t − 1) and x(t + 1) was used to replace x(t). If only one observation (either x(t − 1) or x(t + 1)) was reliable and x(t) was unreliable, we used that observation to replace x(t). Step 2 addresses the situation with two consecutive bad-quality observations ((x(t), x(t + 1)). We defined a filter with a 4-observation moving window (x(t − 1), x(t), x(t + 1), x(t + 2)). We calculated the difference between x(t − 1) and x(t + 2) values and added them as an increment to gap-fill x(t) and

Table 1
A summary description of the two savanna woodland flux tower sites.

Site name	Country (°)	Latitude (°)	Longitude	Ecosystem	C3/C4	MAP (mm)	MAT (°C)	Flux measurements
Maun	Botswana	−19.9155	23.5603	*Mopane* woodland	80/20	464	22.6	1999–2001
Mongu	Zambia	−15.4388	23.2525	*Miombo* woodland	95/5	945	25	2007–2009

MAP: mean annual precipitation; MAT: mean annual temperature.

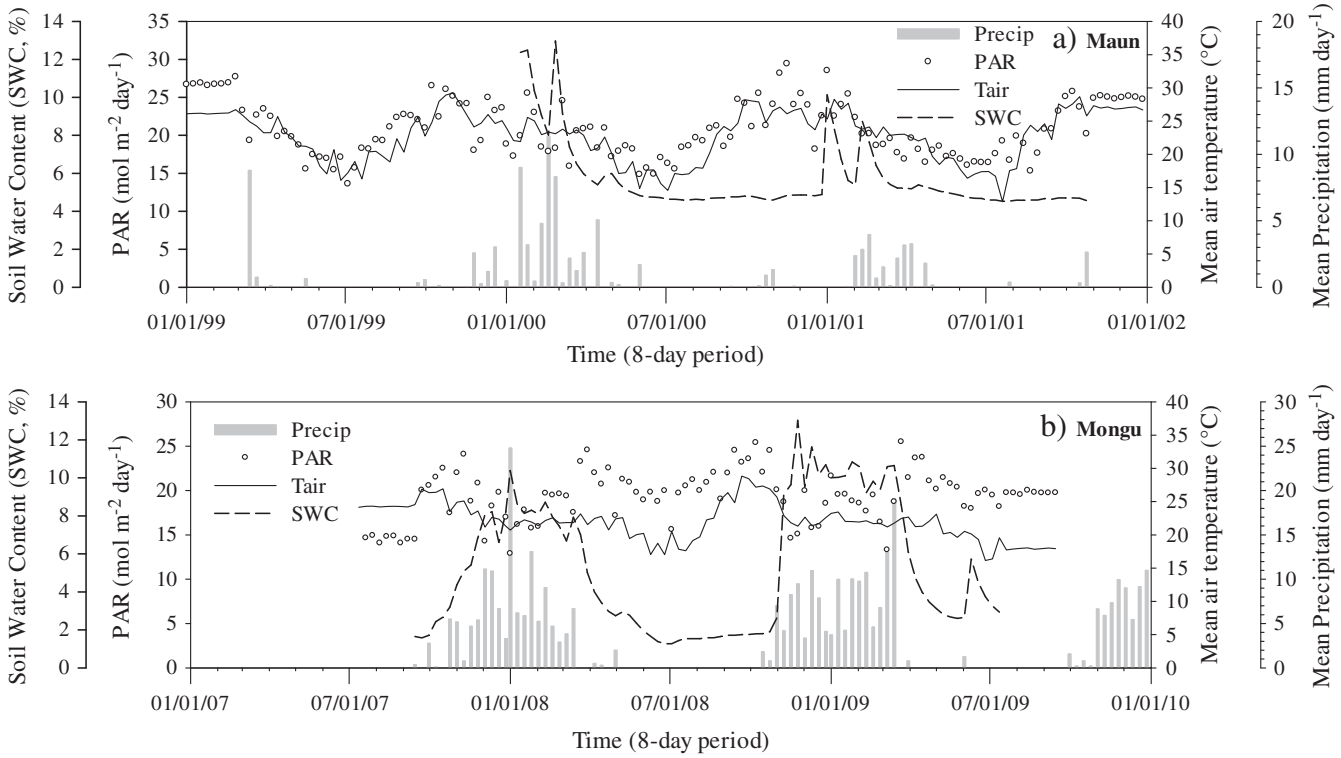

Fig. 2. Seasonal dynamics and interannual variations of precipitation (Precip), photosynthetically active radiation (PAR), soil water content at the upper 100 cm of soil (SWC), and air temperature (T_{air}) observed at the two savanna woodland flux tower sites in Southern Africa. (a) the Maun site, Botswana, during 1999–2001; (b) the Mongu site, Zambia, during 2007–2009.

x(t + 1). Step 3 deals with the situation with three or more consecutive bad observations. We used multi-year mean vegetation index data during 2000–2011 to gap-fill those individual 8-day periods with bad quality. For example, the mean (M) and standard deviation (SD) of NDVI at individual 8-day periods over 2000–2011 (12 years) were first calculated using the reliable observations in 8-day periods, which constructed a mean NDVI time series in a mean year. We then calculated differences of NDVI between reliable observations in a year (e.g., 2007) and the mean NDVI values (M) over 2000–2011 (i.e., the mean year). If a year was closer to the mean year, we used M values to

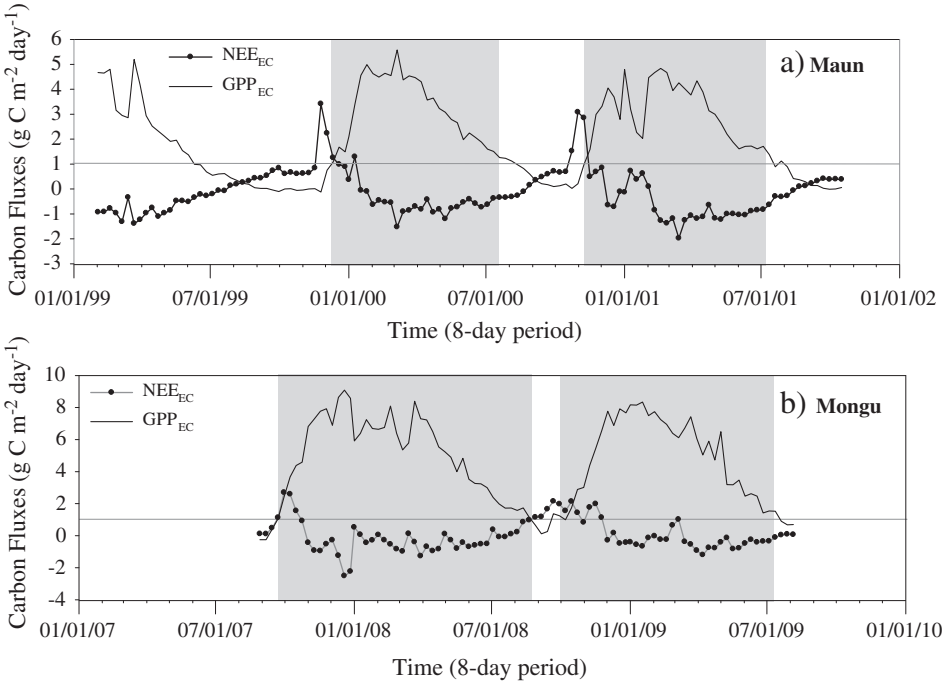

Fig. 3. Seasonal dynamics and interannual variations of observed net ecosystem exchange of CO_2 (NEE_{EC}) and estimated GPP from flux measurements (GPP_{EC}) at the two savanna woodland flux tower sites in Southern Africa, with the growing seasons highlighted. (a) the Maun site, Botswana, during 1999–2001; (b) the Mongu site, Zambia, during 2007–2009.

gap-fill those three or more unreliable observations. If a year was close to the M − SD values, we used M − SD values to gap-fill those three or more unreliable observations. The same rule was applied to M + SD case. Fig. 4 shows a comparison between the raw vegetation index data and the gap-filled vegetation index data at these two sites. 16% and 35% of the vegetation index observations were gap-filled during the growing seasons of the study periods for the Maun and Mongu sites, respectively.

The MODIS GPP product (MOD17A2) was included in this study for the model comparison. MOD17A2 for the two sites was acquired from the Oak Ridge National Laboratory's Distributed Active Archive Center website (http://daac.ornl.gov/MODIS/). MOD17A2 is the continuous remote sensing-driven GPP datasets across the global at a 1-km spatial resolution and an 8-day temporal resolution since 2000. The algorithm that MOD17A2 uses to estimate GPP is (Zhao et al., 2006):

$$GPP = \varepsilon \times FPAR_{canopy} \times PAR \tag{4}$$

where PAR is the photosynthetically active radiation calculated by $0.45 \times S_{\downarrow s}$ ($S_{\downarrow s}$: downward surface solar shortwave radiation), $FPAR_{canopy}$ is the fraction of PAR absorbed by the canopy and obtained from MODIS FPAR/LAR product (MOD15A2), and ε is the light use efficiency and estimated with:

$$\varepsilon = \varepsilon_{max} \times T \times VPD \tag{5}$$

where ε_{max} is the maximum light use efficiency predefined in a Biome Properties Look-Up Table (BPLUT). T and VPD are daily minimum temperature and vapor pressure deficits scalars, respectively. Air temperature, VPD, and $S_{\downarrow s}$ are obtained from the NASA's Data Assimilation Office (DAO).

2.4. The Vegetation Photosynthesis Model (VPM)

The Vegetation Photosynthesis Model (VPM) is based on the conceptual partitioning of chlorophyll and non-photosynthetically active vegetation (NPV) in a canopy. It estimates GPP over the plant growing season at daily or weekly intervals (Xiao et al., 2004b):

$$GPP = \varepsilon \times FPAR_{chl} \times PAR \tag{6}$$

where PAR is the photosynthetically active radiation (μmol photosynthetic photon flux density, PPFD), $FPAR_{chl}$ is the fraction of PAR absorbed by chlorophyll in the canopy, and ε is the light use efficiency (μmol/μmol PPFD).

ε is estimated by the theoretical maximum light use efficiency (ε_{max}, μmol/μmol PPFD), air temperature (T_{scalar}), water condition of land surface (W_{scalar}) and vegetation growing stage (P_{scalar}):

$$\varepsilon = \varepsilon_{max} \times T_{scalar} \times W_{scalar} \times P_{scalar}. \tag{7}$$

T_{scalar} is estimated at each time interval, using the formula developed for the Terrestrial Ecosystem Model (Raich et al., 1991):

$$T_{scalar} = \frac{(T-T_{min})(T-T_{max})}{[(T-T_{min})(T-T_{max})]-\left(T-T_{opt}\right)^2} \tag{8}$$

where T_{min}, T_{opt}, and T_{max} are minimum, optimum, and maximum temperature for leaf photosynthetic activities, respectively. When air temperature falls below T_{min}, T_{scalar} is set to zero. Considering optimum temperature ranges and the predominant climate at the two sites, the T_{min}, T_{opt}, and T_{max} were set to 10 °C, 28 °C, and 48 °C, respectively (McGuire et al., 1992).

Instead of using soil moisture and/or water vapor pressure deficit, the VPM uses LSWI to estimate the effect of land surface water conditions on photosynthesis (W_{scalar}):

$$W_{scalar} = \frac{1-LSWI}{1+LSWI_{max}} \tag{9}$$

where $LSWI_{max}$ is the maximum LSWI during the growing season for an individual pixel (Xiao et al., 2004b). Eq. (9) was proven to work well in vegetation with semi-humid and humid climate (Xiao et al., 2004a, 2004b, 2005b, 2006) and we used it for the Mongu site in this study. LSWI of vegetation under arid and semi-arid climate could have very low values (−0.20 or lower). LSWI threshold value ($LSWI >= -0.1$) was used to delineate vegetation phenology in a dynamic system of bare soils and crops (John et al., 2013; Kalfas et al., 2011). We proposed a slightly modified W_{scalar} (see Eq. 10) and

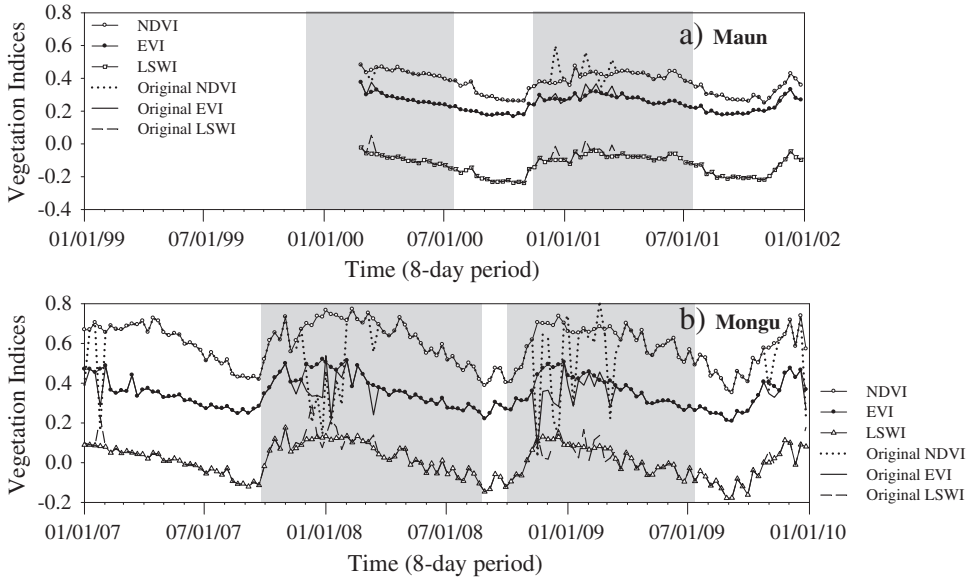

Fig. 4. Seasonal dynamics and interannual variations of three MODIS-derived vegetation indices at the two savanna woodland flux tower sites in Southern Africa, with the growing seasons highlighted (a) the Maun site, Botswana, during 1999–2001; (b) the Mongu site, Zambia, during 2007–2009.

used it for the Maun site (the semi-arid site). In Eq. (10), we added the absolute value of LSWI > = −0.1 into the denominator:

$$W_{scalar} = \frac{1-LSWI}{1+0.1+LSWI_{max}}. \quad (10)$$

P_{scalar} accounts for the effect of leaf longevity on photosynthesis on the canopy level. For deciduous trees, P_{scalar} is calculated at two different phases as linear function:

$$P_{scalar} = \frac{1+LSWI}{2} \quad \text{during bud emergence to full leaf expansion} \quad (11)$$

$$P_{scalar} = 1 \quad \text{after full leaf expansion}. \quad (12)$$

$FPAR_{chl}$ is estimated as a linear function of EVI and the coefficient *a* is set to 1.0 in the current version of the VPM model (Xiao et al., 2004b):

$$FPAR_{chl} = a \times EVI. \quad (13)$$

3. Results

3.1. Land surface phenology as delineated by CO_2 flux data and vegetation indices

3.1.1. The Maun site

GPP_{EC} showed strong seasonal dynamics at the site (Fig. 3a). GPP_{EC} started to rise and exceeded 1 g C m^{-2} day^{-1} in late November 1999, increased rapidly and peaked in March 2000. After the peak, GPP_{EC} gradually decreased and fell below 1 g C m^{-2} day^{-1} again by July 2000. Similar seasonal dynamics also occurred in 2000/2001. The leaf-on and leaf-off phases of mopane woodlands delineated by seasonal GPP_{EC} occurred in November and July, respectively.

At the end of the dry season in 1999/2000, NDVI, EVI, and LSWI remained low (<0.3, <0.2, and <−0.15) for about three months, followed by a rapid increase in early November of 2000/2001 (Fig. 4a). The thresholds of NDVI, EVI, and LSWI, when GPP_{EC} was above 1 g C m^{-2} day^{-1}, were ≥0.3, ≥0.2 and ≥−0.15 (Fig. 4a). All three vegetation indices continuously increased to the maximum in late February. At the end of the wet season, when GPP_{EC} began to decline to 1 g C m^{-2} day^{-1} and below, NDVI, EVI and LSWI decreased similarly (0.3, 0.2, and −0.1) during the leaf senescence and abscission stages. Therefore, compared with the seasonal dynamics and interannual variation of GPP_{EC}, all three vegetation indices have the potential to identify the growth dynamics of mopane woodlands at the Maun site.

Table 2 summarizes the land surface phenology (leaf-on and leaf-off dates) as determined from GPP_{EC} and vegetation indices at the Maun site. As defined by GPP_{EC} (> 1 g C m^{-2} day^{-1}), the leaf-on and leaf-off dates of 2000/2001 were 11/08/2000 and 07/12/2001, respectively. The leaf-on date of 2000/2001 defined by LSWI was the same as defined by GPP_{EC} (11/08/2000); and the leaf-off date defined by LSWI (07/04/2000) differed from that defined by GPP_{EC} (07/12/2001) by one week earlier. The total GPP over the growing season defined by LSWI (710 g C m^{-2}) was about 1.5% lower than the total GPP over the growing season defined by GPP_{EC} (721 g C m^{-2}).

3.1.2. The Mongu site

GPP_{EC} had a strong seasonal dynamics at the site (Fig. 3b), varying between 0 and 9 g C m^{-2} day^{-1}. GPP_{EC} started to rise and exceeded 1 g C m^{-2} day^{-1} in late-September 2007, and rapidly increased until peaking in December 2007 (Fig. 3b). From June to August 2008, GPP_{EC} continuously decreased and reached 1 g C m^{-2} day^{-1}. Similar temporal dynamics occurred in 2008/2009. Therefore, the leaf-on phase began in September, and the leaf-off phase happened between June and August.

NDVI, EVI, and LSWI increased in late September and corresponded well with the timing of GPP_{EC} increase. The thresholds of NDVI, EVI, and LSWI, when GPP_{EC} was above 1 g C m^{-2} day^{-1}, were ≥0.4, ≥0.3, and ≥−0.1, respectively (Fig. 4b). NDVI, EVI, and LSWI peaked between November and January, and slowly decreased afterwards to 0.4/0.5, 0.3, and −0.1. The leaf-on and leaf-off dates defined by LSWI (≥−0.1) in 2007/2008 were the same as defined by GPP_{EC} (Table 2), and the total GPP over the growing season defined by LSWI (1789 g C m^{-2}) was the same amount as the total GPP_{EC}. For 2008/2009, the leaf-on date defined by LSWI was one 8-day interval later than the one defined by GPP_{EC} whereas the leaf-off date was one 8-day interval earlier than the one defined by GPP_{EC}. The total GPP over the growing season defined by LSWI (1486 g C m^{-2}) was 1.5% lower than the total GPP over the growing season defined by GPP_{EC} (1510 g C m^{-2}).

3.2. Quantitative relationships between vegetation indices and GPP_{EC}

At the Maun site, simple linear regression models between vegetation indices (NDVI and EVI) and GPP_{EC} during the growing season (LSWI ≥ −0.15 or −0.1) show that NDVI and EVI accounted for 22% and 67% of GPP_{EC} variances, respectively (Fig. 5a, b). Due to the sparse vegetation coverage with maximum leaf area index of 1.0 at the Maun site, NDVI can be easily influenced by soil background (Huete et al., 2002). Thus, the weak linear relationship between NDVI and GPP_{EC} can be attributed to the NDVI sensitivity to soil background under the low vegetation coverage at the Maun site. EVI performs better to track the subtle changes of mopane woodlands at this site by correcting the impact of canopy background and atmosphere correction (Huete et al., 2002).

At the Mongu site, NDVI and EVI accounted for 65% and 68% of GPP_{EC} variances, respectively (Fig. 5c, d). EVI had a slightly stronger linear relationship with GPP_{EC} than NDVI. The relatively weak linear relationship between NDVI and GPP_{EC} might be attributed to the NDVI saturation in dense canopies as found at the Mongu site. During the peak of growing season (GPP_{EC} > 6 g C m^{-2} day^{-1}), NDVI values

Table 2
Land surface phenology (leaf-on and Leaf-off dates) of the savanna woodland flux tower sites in Botswana and Zambia, as delineated by the estimated GPP from the flux towers (GPP_{EC}) and a NIR/SWIR-based vegetation index (LSWI).

Site name	GPP_{EC} ≥ 1 g C m^{-2} day^{-1}		Total GPP_{EC}	LSWI ≥ −0.1 or ≥−0.15[a]		Total GPP_{EC}	GPP_{EC} %RE
	Leaf-on date	Leaf-off date		Leaf-on date	Leaf-off date		
Maun	12/11/2000	07/19//2000		N/A	07/11/2000[a]	N/A	N/A
	11/8/2000	07/12/2001	721	11/8/2000[a]	07/04/2001	710	−1.5%
Mongu	09/22/2007	08/20/2008	1789	09/22/2007	08/20/2008	1789	0%
	09/21/2008	07/12/2009	1510	09/29/2008	07/04/2009	1486	−1.5%

[a] If LSWI time series data have values of <−0.15, we chose LSWI threshold value to be ≥−0.15. Starting date for LSWI was the first date that has consecutive LSWI values ≥−0.1/−0.15 over the period of late dry season to early wet season; Ending date for LSWI was the first date that has LSWI values ≥−0.1/−0.15 over the period of late wet season and early dry season.

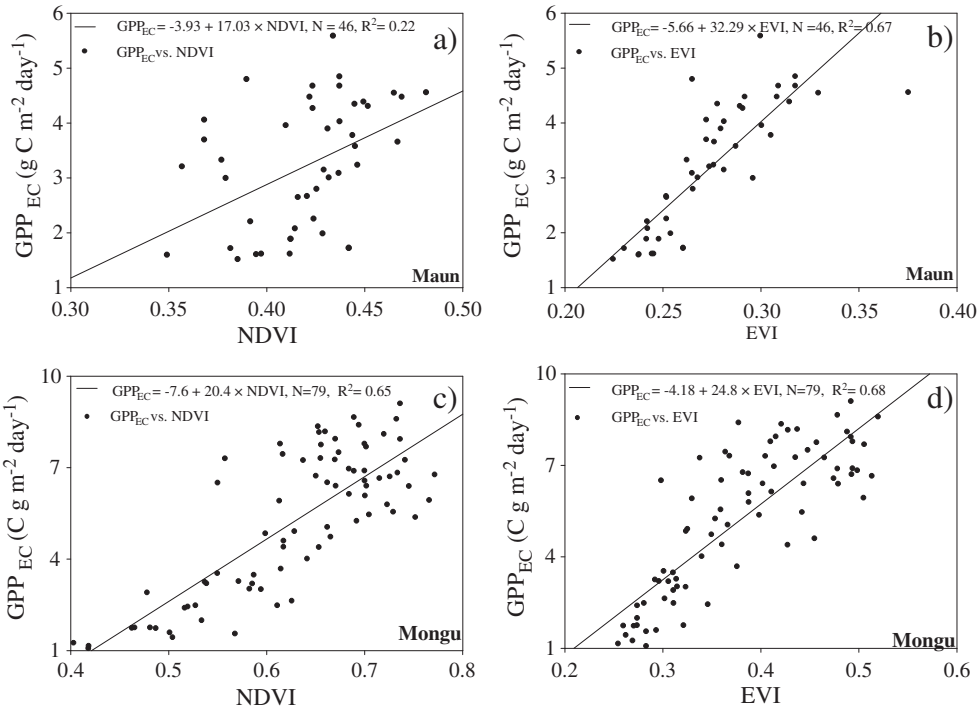

Fig. 5. Relationships between two vegetation indices (NDVI, EVI) and estimated GPP from the flux tower data (GPP_{EC}) during the growing seasons at the two savanna woodland flux tower sites in Southern Africa. (a) and (b) the Maun site, Botswana, during 1999–2001; (c) and (d) the Mongu site, Zambia, during 2007–2009.

concentrated from 0.7 to 0.8. However, EVI had the wider dynamic range of 0.3–0.5 and was more sensitive to the canopy changes of miombo woodlands.

Note that NDVI accounted for 22% of GPP_{EC} variance at the Maun site but 65% of GPP_{EC} at the Mongu site. This large discrepancy in biophysical performance is attributed to the sensitivity of NDVI to soil background. LAI was much higher at the Mongu site than at the Maun site (see Section 2.1). This clearly suggests that for the study of sparse vegetation in arid and semi-arid climates, one needs to be cautious when using NDVI to estimate biophysical parameters such as GPP.

3.3. Seasonal dynamics of GPP from the Vegetation Photosynthesis Model (GPP_{VPM})

3.3.1. The Maun site

The seasonal dynamics of GPP_{VPM} corresponded well with GPP_{EC} over the period of February to July 2000 (Fig. 6). The simple linear correlation analysis between GPP_{VPM} and GPP_{EC} showed that GPP_{VPM} was strongly correlated with GPP_{EC} during this period ($R^2 = 0.92$, $p < 0.001$, Fig. 7a). The root mean square deviation value (RMSD) was 0.32 g C m^{-2} day^{-1} in 1999/2000 (Table 3). The sum of GPP_{VPM} over the period with observations available was 468 g C m^{-2}, which was about 0.6% higher than the sum of GPP_{EC} (465 g C m^{-2}).

During 2000/2001, the seasonal dynamics of GPP_{VPM} tracked reasonably well with GPP_{EC} except in January and July 2001 (Fig. 6). The simple linear regression model between GPP_{VPM} and GPP_{EC} in 2000/2001 had a slope of 1.02 but $R^2 = 0.64$ ($p < 0.001$, Fig. 7b), which suggested that GPP_{EC} data in 2001 had much larger variation. The RMSD value was 0.67 g C m^{-2} day^{-1} in 2000/2001 (Table 3). The seasonal sum of GPP_{VPM} in 2000/2001 was 753 g C m^{-2}, being 6.1% higher than the seasonal sum of GPP_{EC} (710 g C m^{-2}).

3.3.2. The Mongu site

The seasonal dynamics of GPP_{VPM} tracked well with GPP_{EC} during 2007/2008 (Fig. 8). GPP_{VPM} started to increase in late-September 2007, and reached the peak in December 2007. GPP_{VPM} decreased gradually after January and fell below 1 g C m^{-2} day^{-1} after July 2008. The

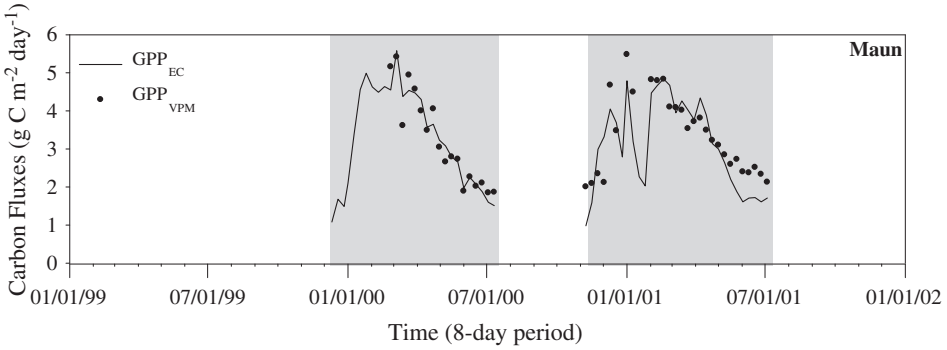

Fig. 6. Seasonal dynamics and interannual variations of GPP at the Maun site, Botswana, during 1999–2001, with the growing seasons highlighted. GPP_{EC} — estimated GPP from the flux tower data; GPP_{VPM} – predicted GPP from the VPM model.

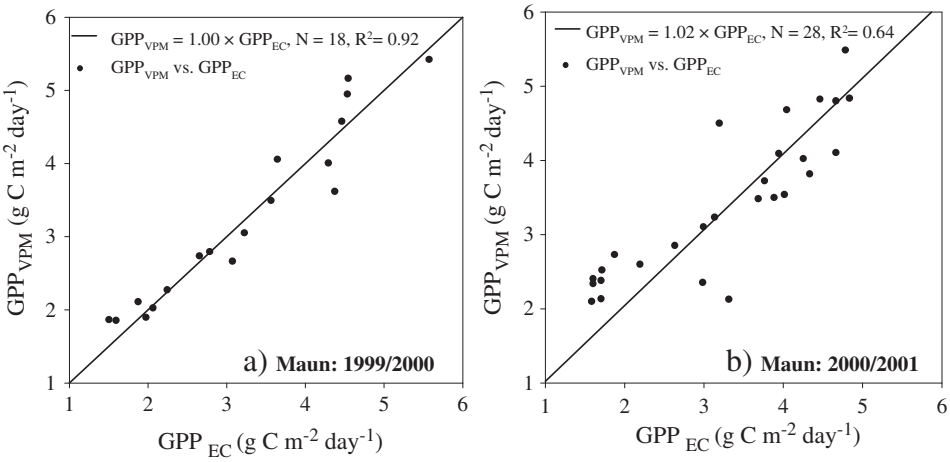

Fig. 7. Comparison between GPP_{EC} and GPP_{VPM} at the Maun site, Botswana, during (a) 1999/2000, (b) 2000/2001.

simple linear correlation analysis showed that GPP_{VPM} correlated well with GPP_{EC} in 2007/2008 ($R^2 = 0.87$, $p < 0.001$, Fig. 9a). The RMSD value was 0.76 g C m^{-2} day^{-1} over the period of 2007/2008. The seasonal sum of GPP_{VPM} during 2007/2008 was 1759 g C m^{-2}, approximately 1.7% lower than the sum of GPP_{EC} (1789 g C m^{-2}).

The seasonal dynamics of GPP_{VPM} in the period of 2008/2009 showed the same trend as in 2007/2008. The simple linear correlation analysis showed that GPP_{VPM} correlated well with GPP_{EC} in 2008/2009 ($R^2 = 0.86$, $p < 0.001$, Fig. 9b). The RMSD value was 0.90 g C m^{-2} day^{-1} over the period of 2008/2009. The seasonal sum of GPP_{VPM} during 2008/2009 was 1422 g C m^{-2}, approximately 4.4% lower than the seasonal sum of GPP_{EC} (1487 g C m^{-2}).

4. Discussion

The importance of phenology of savanna woodlands in relation to the seasonal variation of net primary production has been recognized in earlier studies (De Bie et al., 1998). Several studies have evaluated and reported on the phenology of savanna vegetation (Chidumayo, 2001; Fuller, 1999; Fuller & Prince, 1996; Hutley et al., 2011; Oliveira et al., 2012; Vrieling et al., 2011; Wagenseil & Samimi, 2006). These studies found that NDVI had strong responses to phenological changes of savanna vegetation (Batista et al., 1997; Franca & Setzer, 1998). For instance, Fuller (1999) and Fuller and Prince (1996) delineated leaf dynamics of savanna woodlands in Africa (including the mopane and miombo woodlands) with time series NOAA/AVHRR NDVI and rainfall data. The thresholds of average NDVI increase of 0.06 and average rainfall of 50 mm during September and October as an indication for vegetation growth status and water content status were pre-defined to retrieve the early greening stage of savanna woodlands in the study (Fuller, 1999; Fuller & Prince, 1996). However, due to the effects of interception, run-off, and soil water movement, the threshold of the rainfall varying over space could not precisely represent the leaf water status. A few recent studies reported that EVI behaved better than NDVI to quantify the leaf dynamics of tropical savanna and could effectively describe the phenology (Bradley et al., 2011; Couto et al., 2011; Ferreira & Huete, 2004; Ferreira et al., 2003; Hoffmann et al., 2005; Hüttich et al., 2009).

In this study we used both an ecosystem–physiology approach and a remote sensing approach to delineate phenology of savanna woodlands, and the results clearly showed the convergence between these two approaches. As shown in this study, EVI threshold values ranged from 0.2 to 0.3, which is smaller than the range of NDVI threshold values (0.3 to 0.5). These results confirmed that EVI was more stable (a smaller range of threshold values used for leaf-on and leaf-off phases) than NDVI for delineating phenology of savanna woodlands when the threshold method was used. In addition, our study also showed that LSWI was more stable than NDVI and EVI for delineating phenology of savanna woodlands. The LSWI threshold value (≥ -0.1) has been used to determine the emergence (leaf-on) and harvest (leaf-off) of croplands (Kalfas et al., 2011; Yan et al., 2009). In recent years, NIR/SWIR-based vegetation indices have received more attention for their potential in evaluating seasonal dynamics of vegetation canopy (Townsend et al., 2012; Xiao et al., 2002).

Simulations of satellite-driven Production Efficiency Models (PEM), including the VPM, are affected by model parameterization and calibration (Wu et al., 2011). Different definitions and choices of maximum light use efficiency (ε_{max}) and environmental factors are the main sources of PEM uncertainties. ε_{max} determines the potential conversion efficiency of absorbed photosynthetically active radiation under the ideal growing condition. The values of ε_{max} should be determined according to the vegetation function types (VFT). Some PEMs defined ε_{max} as an global constant value for all vegetation types; and others used the theoretical values from experiment measurements; and some derived ε_{max} from the model fitting between NEE and PAR during the peak of growing season (Chen et al., 2011; Goerner et al., 2011; Wang et al., 2010a; Wu & Niu, 2012; Xiao et al., 2006; Zhu et al., 2006).

The theoretical ε_{max} of C_3, 0.9 g C mol $PPFD^{-1}$ (Ehleringer & Björkman, 1977) used in this simulation, is higher than the value of 0.63 g C mol $PPFD^{-1}$ (or 1.29 g C MJ^{-1}) used by a previous study of tropical savanna in Northern Australia(Kanniah et al., 2009, 2011), and the value of 1.21 g C MJ^{-1} (or 0.484 g C mol $PPFD^{-1}$) used in the standard MODIS algorithm (MOD17A2) for the Maun site and the Mongu site (Sjöström et al., 2013). The large variation

Table 3
A summary of GPP estimated from the flux towers (GPP_{EC}) and the predictions from the VPM model (GPP_{VPM}) at the savanna woodland flux tower sites in Botswana and Zambia. GPP_{EC}: seasonal sum of GPP estimated from the eddy covariance flux tower observations in g C m^{-2}, GPP_{VPM}: seasonal sum of GPP predicted by the VPM in g C m^{-2}, GPP%RE: relative error in GPP sums calculated as $[(GPP_{VPM} - GPP_{EC})/GPP_{EC}] \times 100$, RMSD: Root mean squared deviation.

Site name	Plant growing season	GPP_{EC}	GPP_{VPM}	GPP%RE	RMSD
Maun	1999–2000[a]	465	468	0.6	0.32
	2000–2001	710	753	6.1	0.67
Mongu	2007–2008	1789	1759	−1.7	0.76
	2008–2009	1487	1422	−4.4	0.90

[a] MODIS data start to be available on 02/26/2000. At the Maun site, data from 02/26/2000 to 07/11/2000 were used.

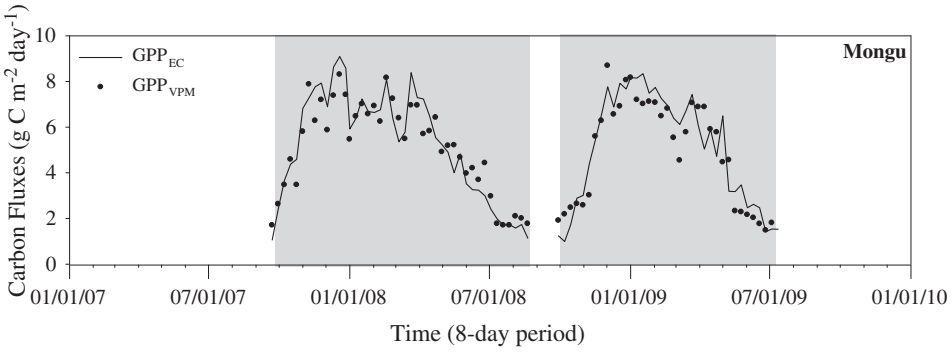

Fig. 8. Seasonal dynamics and interannual variations of GPP_{EC} and GPP_{VPM} at the Mongu site, Zambia, during 2007–2009, with the growing seasons highlighted.

of ε_{max} values in the PEMs suggests that more investigations of light use efficiency calculation for savanna ecosystems, the mixed biome of tree (C_3) and grass (C_4), are needed. Accurate estimation of light use efficiency of the tree and grass mixed ecosystems needs precise experiments and modeling of the physiological and biochemical processes on the stand, canopy, and landscape scales (Caylor & Shugart, 2004; Ludwig et al., 2004; Scholes & Archer, 1997; Skarpe, 1992; Whitley et al., 2011).

The VPM uncertainties also come from the two dominant down-regulation environmental factors related to water (W_{scalar}) and temperature (T_{scalar}). Here we report a model sensitivity analysis of the VPM: (1) without W_{scalar} ($GPP_{VPM\_w/o\_Wscalar}$), (2) without T_{scalar} ($GPP_{VPM\_w/o\_Tscalar}$), and (3) without both W_{scalar} and T_{scalar} ($GPP_{VPM\_w/o\_Wscalar\_Tscalar}$) (Figs. 10, 11, Table 4). The effect of W_{scalar} on GPP_{VPM} is relatively larger at the Maun site than at the Mongu site, which is likely related to lower annual precipitation at the Maun site (464 mm, semi-arid climate) than at the Mongu site (945 mm, semi-humid climate). The effect of T_{scalar} on GPP_{VPM} is also much larger at the Maun site than at the Mongu site, which is likely related to the range of temperature variation at these sites (see Fig. 2). When we compared the changes in slope ($GPP_{VPM} = a \times GPP_{EC}$), W_{scalar} had a higher impact than T_{scalar}. When we compared the changes in R^2, W_{scalar} had less impact than T_{scalar}. In the case without both T_{scalar} and W_{scalar}, the model overestimated GPP by 46% to 50% at the Maun site and by 13% to 16% at the Mongu site, suggesting that it is important to consider both water and temperature to downscale maximum light use efficiency when estimating the GPP with PEMs in semi-arid climate.

At the Maun site, the discrepancy between GPP_{VPM} and GPP_{EC} seems relatively large in 2000/2001. This could be explained by MODIS data and GPP_{EC} data. One example is that GPP_{EC} in January 2001 dropped to 2 g C m^{-2} day^{-1} (Fig. 6), more than 100% lower than the GPP_{EC} value in December 2000. Note that soil moisture data in January 2001 also had a dramatic drop (Fig. 2a) but NEE data had a dramatic increase (Fig. 3a). As soil moisture data were used to estimate ecosystem respiration, consequently GPP_{EC} dropped substantially in January 2001. However, the three vegetation indices did not drop accordingly in January 2001(Fig. 4a). If these observations of soil moisture and NEE data in January 2011 had no quality problem, one can speculate that the three vegetation indices are not able to reflect how short-term drought (flash drought) affected the vegetation. Another example is the discrepancy between GPP_{VPM} and GPP_{EC} in late May to June 2001. All three vegetation indices were higher in late May and June 2001 than in April to early May, but soil moisture and precipitation data did not support the short-term increases in vegetation indices in that period. As the 8-day MODIS composite images were used in this study, evaluation of the image compositing method using daily MODIS images in semi-arid climates might be needed in the future.

The comparisons between the MODIS GPP product ($GPP_{MOD17A2}$) with GPP_{EC} have shown that $GPP_{MOD17A2}$ overestimated GPP at the Maun site, and underestimated GPP at the Mongu site (Sjöström et al., 2011, 2013). Here we compared seasonal dynamics and interannual variation of $GPP_{MOD17A2}$ and GPP_{VPM} (Fig. 12). At the Maun site, $GPP_{MOD17A2}$ was substantially lower than GPP_{EC} during the first half of the growing season but higher than GPP_{EC} during the second half of the growing season (Fig. 12a). At the Mongu site, $GPP_{MOD17A2}$ was substantially lower (up to 50%) than GPP_{EC} throughout the entire growing season (Fig. 12b). In Wu et al. (2010), the underestimation of two PEMs (the VPM and MOD17A2) happened among multiple-year simulations at a deciduous forest site. At the

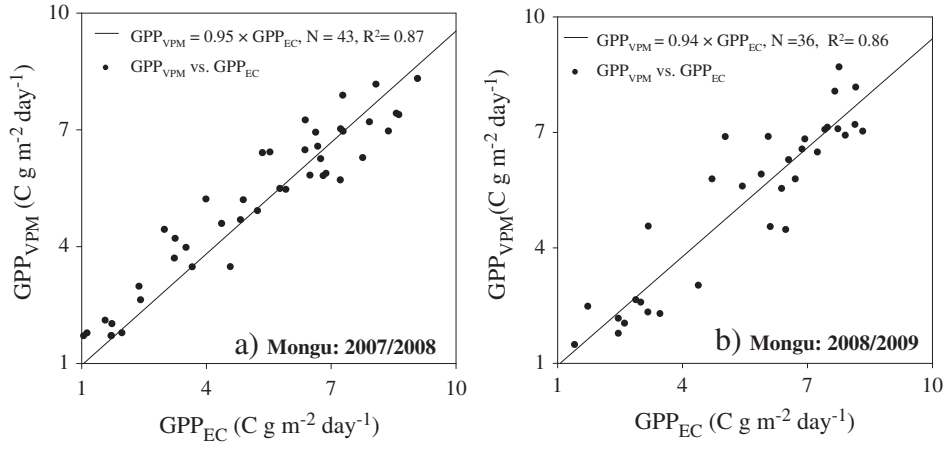

Fig. 9. Comparison between GPP_{EC} and GPP_{VPM} at the Mongu site, Zambia, during (a) 2007/2008, (b) 2008/2009.

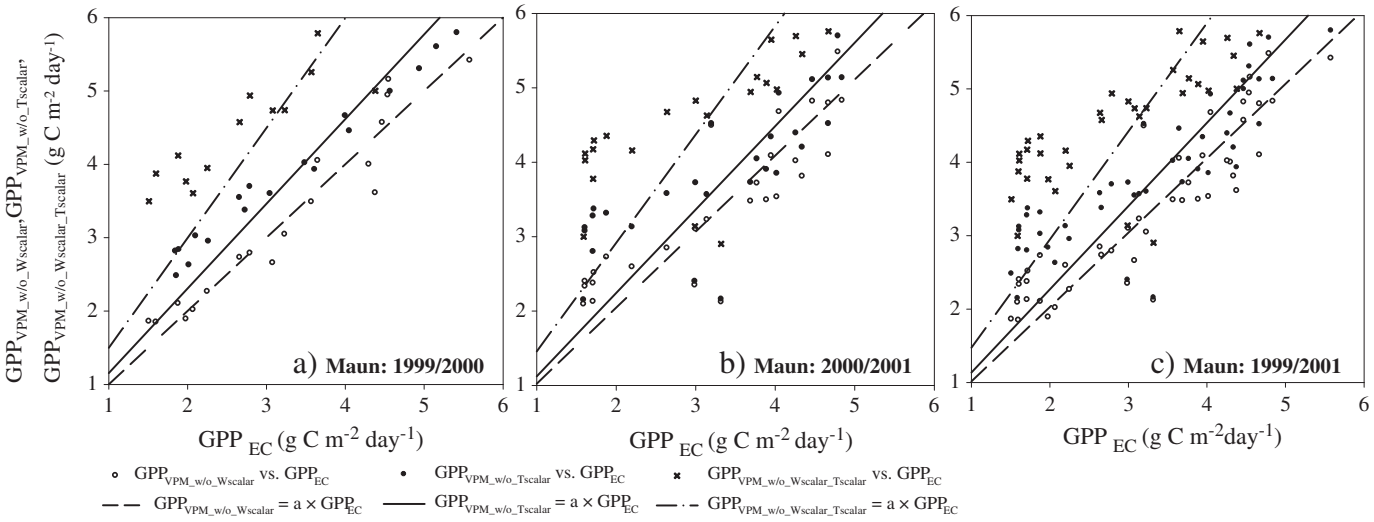

Fig. 10. Sensitivity analysis of the VPM model at the Maun site, Botswana. It includes three cases of VPM simulations related to W_{scalar} and T_{scalar}: (1) without W_{scalar}, i.e., $\varepsilon = \varepsilon_{max} \times T_{scalar} \times P_{scalar}$; (2) without T_{scalar}, i.e., $\varepsilon = \varepsilon_{max} \times W_{scalar} \times P_{scalar}$; and (3) without both W_{scalar} and T_{scalar}, i.e., $\varepsilon = \varepsilon_{max} \times P_{scalar}$. (a) 1999/2000 season; (b) 2000/2001 season; (c) both 1999/2000 and 2000/2001 seasons. See also Table 4 for the slopes and R^2 values of individual simple linear regression models.

Mongu site in our study, it was found that both the GPP simulation from the VPM (GPP_{VPM}) and MOD17A2 ($GPP_{MOD17A2}$) at this site were underestimated compared to GPP_{EC}, especially for $GPP_{MOD17A2}$ (Fig. 12b) which is consistent with the result from Wu et al. (2010). A possible explanation might be that MODIS sensors are not able to sense the shaded leaves within the canopy, since the Mongu site is located in the Kataba Forest Reserve with a dense tree canopy, high LAI (the canopy height is above 10 m with the fractional canopy cover of 67%) and very sparse understory vegetation (Section 2.1 and Fig. 1c), and might be defined as "forest" to some degree. At the Maun site, both GPP_{VPM} and $GPP_{MOD17A2}$ didn't show the significant underestimation compared with the Mongu site, and were closed to GPP_{EC} (slightly overestimated, Fig. 12a). The Maun is characterized as a sparse woodland, with a canopy height of 5–10 m and fractional canopy cover of 36%. In this situation, the MODIS sensors may sense all leaves within the canopy. In addition, other factors, such as global climate datasets used in MOD17A2 product, maximum light use efficiency parameter, and the fraction of photosynthetic active radiation absorbed by vegetation canopy ($FPAR_{canopy}$) further contribute to the large discrepancies between $GPP_{MOD17A2}$ and GPP_{EC} (Wu et al., 2010). Detailed analysis of the MOD17A2 algorithm is beyond the scope of this paper, but it does suggest that validation of satellite-driven PEMs at individual flux tower sites of savanna woodlands is important.

Savanna woodlands are widely distributed in the world, and GPP estimates from various publications vary substantially in different countries and continents. For example, GPP estimates ranged from 576 g C m^{-2} in semi-arid savanna to 1680 g C m^{-2} mesic savanna woodlands in Northern Australia (Hutley et al., 2005; Kanniah et al., 2011). GPP estimates varied from approximately 900–1380 g C m^{-2} for deciduous oak and grass savanna in California, USA (Ma et al., 2007) to 1300–2200 g C m^{-2} for evergreen oak and grass savanna in Portugal (Pereira et al., 2007). Only a few publications have reported the use of the PEMs and MODIS data for estimating GPP in

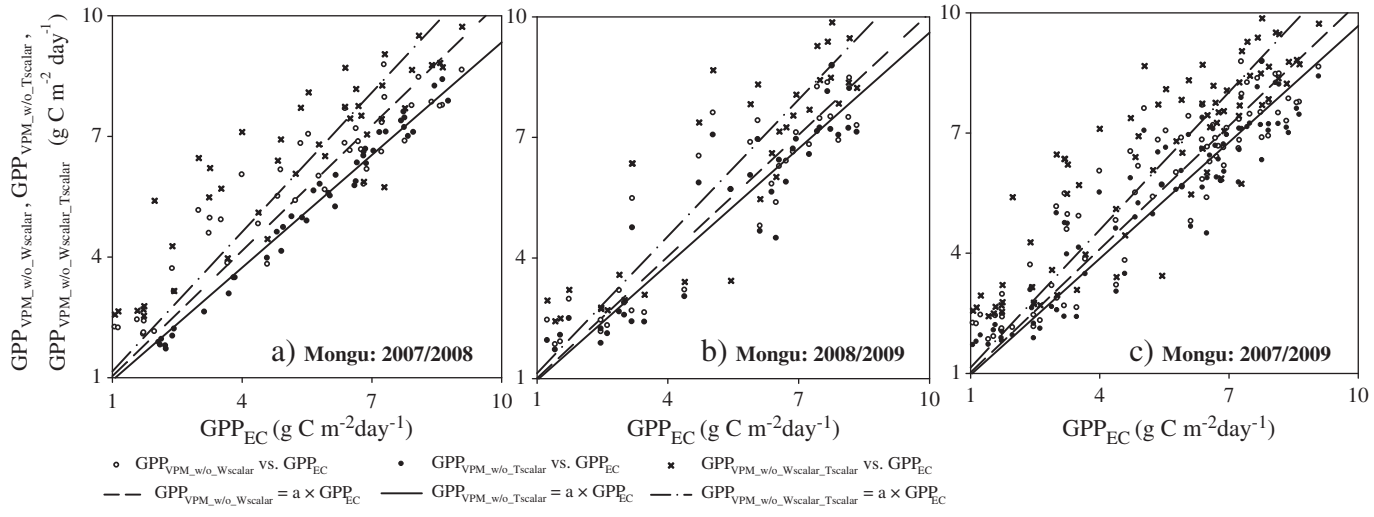

Fig. 11. Sensitivity analysis of the VPM model at the Mongu site, Zambia, including three cases of VPM simulations related to W_{scalar} and T_{scalar}: (1) without W_{scalar}, i.e., $\varepsilon = \varepsilon_{max} \times T_{scalar} \times P_{scalar}$; (2) without T_{scalar}, i.e., $\varepsilon = \varepsilon_{max} \times W_{scalar} \times P_{scalar}$; and (3) without both W_{scalar} and T_{scalar}, i.e., $\varepsilon = \varepsilon_{max} \times P_{scalar}$. (a) 2007/2008 season; (b) 2008/2009 season; (c) both 2007/2008 and 2008/2009 seasons. See also Table 4 for the slopes and R^2 values of individual simple linear regression models.

Table 4
A summary of model sensitivity analysis for the VPM model, including three cases of VPM simulations related to W_{scalar} and T_{scalar}: (1) without W_{scalar}, i.e., $\varepsilon = \varepsilon_{max} \times T_{scalar} \times P_{scalar}$; (2) without T_{scalar}, i.e., $\varepsilon = \varepsilon_{max} \times W_{scalar} \times P_{scalar}$; and (3) without both W_{scalar} and T_{scalar}, i.e., $\varepsilon = \varepsilon_{max} \times P_{scalar}$.

Site	Year	$GPP_{VPM} = a \times GPP_{EC}$		$GPP_{VPM\_w/o\_Wscalar} = a \times GPP_{EC}$		$GPP_{VPM\_w/o\_Tscalar} = a \times GPP_{EC}$		$GPP_{VPM\_w/o\_Wscalar\_Tscalar} = a \times GPP_{EC}$	
		a	R^2	a	R^2	a	R^2	a	R^2
Maun	1999/2000	1	0.92	1.17	0.91	1.15	0.73	1.50	0.55
	2000/2001	1.02	0.64	1.20	0.57	1.12	0.30	1.46	0.18
Mongu	2007/2008	0.95	0.87	1.00	0.80	0.97	0.83	1.16	0.61
	2008/2009	0.94	0.86	1.04	0.79	0.96	0.85	1.13	0.76

savanna woodlands (Kanniah et al., 2011, 2009; Sjöström et al., 2011). Evaluation of MODIS-based vegetation indices and the VPM model at these different savanna woodland ecosystems in the world would provide additional insight on vegetation phenology, biophysical performance of vegetation indices, and performance of the VPM model in savanna woodland ecosystems.

5. Conclusion

The information of land surface phenology growing season length is useful for simulations of satellite-based PEMs. In this study, the land surface phenology of savanna woodlands, described by the satellite vegetation indices, especially the NIR/SWIR–water-sensitive vegetation indices (e.g., LSWI), was proven to agree well with the phenology based on ecosystem physiology as measured by eddy covariance technique. Previous studies have shown that the Vegetation Photosynthesis Model (VPM) provides robust and reliable estimates of GPP across several biomes and geographic regions. This study has also demonstrated the potential of the VPM to estimate the GPP in two savanna woodland ecosystems in Southern Africa. The simulation results showed that the VPM performs reasonably well in tracking the seasonal dynamics and interannual variation of GPP at these two savanna woodland sites. Further evaluation of the VPM simulations for other savanna vegetation types is necessary before it is applied to estimate GPP of savanna ecosystems in Southern Africa at regional and continental scales.

Acknowledgments

This work was supported by a research grant from the NASA Earth Observing System (EOS) Data Analysis Program (NNX09AE93G), and a research grant from the National Science Foundation (NSF) EPSCoR program (NSF-0919466). MODIS MOD09A1 data products are distributed by the Land Processes Distributed Active Archive Center (LP DAAC), located at the US Geological Survey (USGS) Earth Resources Observation and Science (EROS) Center (http://lpdaac.usgs.gov). Site-specific climate and CO_2 flux data from the Maun and Mongu sites were obtained with financial support from the CarboAfrica Initiative (EU, Contract No: 037132) and the Max-Planck Institute for Biogeochemistry, Jena, Germany. We thank two reviewers for their insightful comments on earlier version of the manuscript. We would also like to thank Melissa L. Scott for the English and grammar corrections.

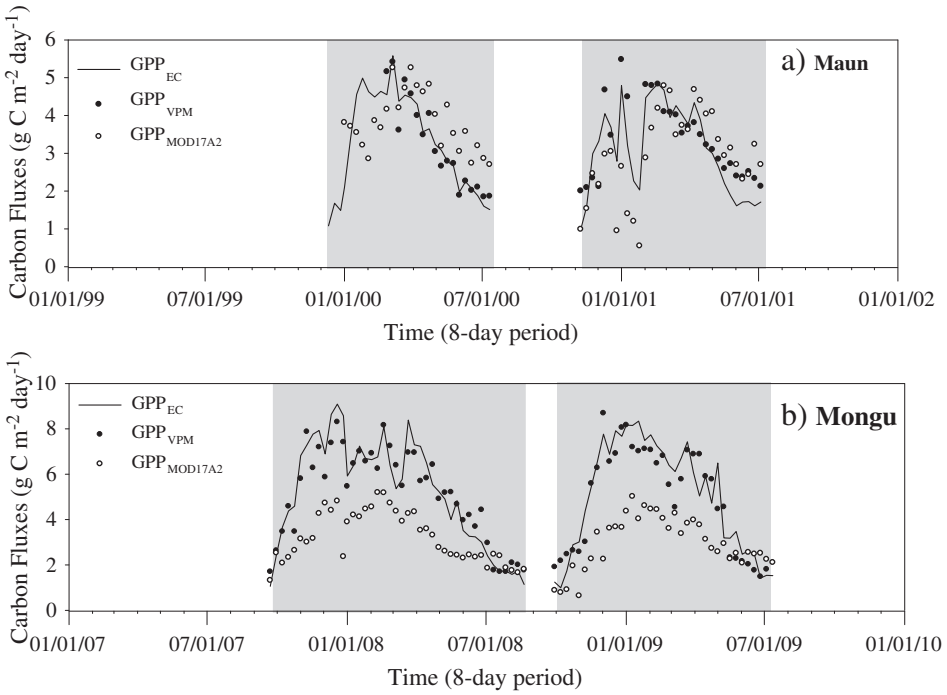

Fig. 12. Comparison of GPP_{EC} and GPP_{VPM} as well as MODIS GPP product ($GPP_{MOD17A2}$). (a) the Maun site, Botswana, during 1999–2001; (b) the Mongu site, Zambia, during 2007–2009.

References

Alcantara, C., Kuemmerle, T., Prishchepov, A. V., & Radeloff, V. C. (2012). Mapping abandoned agriculture with multi-temporal MODIS satellite data. *Remote Sensing of Environment*, *124*, 334–347.

Archibald, S. A., Kirton, A., van der Merwe, M. R., Scholes, R. J., Williams, C. A., & Hanan, N. (2009). Drivers of inter-annual variability in net ecosystem exchange in a semi-arid savanna ecosystem, South Africa. *Biogeosciences*, *6*, 251–266.

Archibald, S., & Scholes, R. J. (2007). Leaf green-up in a semi-arid African savanna — Separating tree and grass responses to environmental cues. *Journal of Vegetation Science*, *18*, 583–594.

Arneth, A., Veenendaal, E. M., Best, C., Timmermans, W., Kolle, O., Montagnani, L., et al. (2006). Water use strategies and ecosystem–atmosphere exchange of CO_2 in two highly seasonal environments. *Biogeosciences*, *3*, 421–437.

Batista, G. T., Shimabukuro, Y. E., & Lawrence, W. T. (1997). The long-term monitoring of vegetation cover in the Amazonian region of northern Brazil using NOAA–AVHRR data. *International Journal of Remote Sensing*, *18*, 3195–3210.

Beer, C., Reichstein, M., Tomelleri, E., Ciais, P., Jung, M., Carvalhais, N., et al. (2010). Terrestrial gross carbon dioxide uptake: Global distribution and covariation with climate. *Science*, *329*, 834–838.

Bradley, A. V., Gerard, F. F., Barbier, N., Weedon, G. P., Anderson, L. O., Huntingford, C., et al. (2011). Relationships between phenology, radiation and precipitation in the Amazon region. *Global Change Biology*, *17*, 2245–2260.

Bradley, B. A., Jacob, R. W., Hermance, J. F., & Mustard, J. F. (2007). A curve fitting procedure to derive inter-annual phenologies from time series of noisy satellite NDVI data. *Remote Sensing of Environment*, *106*, 137–145.

Brown, M. E., de Beurs, K. M., & Marshall, M. (2012). Global phenological response to climate change in crop areas using satellite remote sensing of vegetation, humidity and temperature over 26 years. *Remote Sensing of Environment*, *126*, 174–183.

Cai, H. Y., Zhang, S. W., Bu, K., Yang, J. C., & Chang, L. P. (2011). Integrating geographical data and phenological characteristics derived from MODIS data for improving land cover mapping. *Journal of Geographical Sciences*, *21*, 705–718.

Caylor, K. K., & Shugart, H. H. (2004). Simulated productivity of heterogeneous patches in Southern African savanna landscapes using a canopy productivity model. *Landscape Ecology*, *19*, 401–415.

Chandrasekar, K., Sesha Sai, M. V. R., Roy, P. S., & Dwevedi, R. S. (2010). Land surface water index (LSWI) response to rainfall and NDVI using the MODIS vegetation index product. *International Journal of Remote Sensing*, *31*, 3987–4005.

Chen, T. X., van der Werf, G. R., Dolman, A. J., & Groenendijk, M. (2011). Evaluation of cropland maximum light use efficiency using eddy flux measurements in North America and Europe. *Geophysical Research Letters*, *38*.

Chidumayo, E. N. (2001). Climate and phenology of savanna vegetation in southern Africa. *Journal of Vegetation Science*, *12*, 347–354.

Ciais, P., Bombelli, A., Williams, M., Piao, S. L., Chave, J., Ryan, C. M., et al. (2011). The carbon balance of Africa: Synthesis of recent research studies. *Philosophical Transactions of the Royal Society A - Mathematical Physical and Engineering Sciences*, *369*, 2038–2057.

Coops, N. (1999). Improvement in predicting stand growth of *Pinus radiata* (D. Don) across landscapes using NOAA AVHRR and Landsat MSS imagery combined with a forest growth process model (3-PGS). *Photogrammetric Engineering and Remote Sensing*, *65*, 1149–1156.

Couto, A. F., de Carvalho, O. A., Martins, E. D., Santana, O. A., de Souza, V. V., & Encinas, J. I. (2011). Denoising and characterization of cerrado physiognomies using MODIS times series. *Revista Arvore*, *35*, 699–705.

De Bie, S., Ketner, P., Paasse, M., & Geerling, C. (1998). Woody plant phenology in the West Africa savanna. *Journal of Biogeography*, *25*, 883–900.

Ehleringer, J., & Björkman, O. (1977). Quantum yields for CO_2 uptake in C3 and C4 plants: Dependence on temperature, CO_2, and O_2 concentration. *Plant Physiology*, *59*, 86–90.

Ferreira, L. G., & Huete, A. R. (2004). Assessing the seasonal dynamics of the Brazilian Cerrado vegetation through the use of spectral vegetation indices. *International Journal of Remote Sensing*, *25*, 1837–1860.

Ferreira, L. G., Yoshioka, H., Huete, A., & Sano, E. E. (2003). Seasonal landscape and spectral vegetation index dynamics in the Brazilian Cerrado: An analysis within the large-scale biosphere–atmosphere experiment in Amazonia (LBA). *Remote Sensing of Environment*, *87*, 534–550.

Franca, H., & Setzer, A. W. (1998). AVHRR temporal analysis of a savanna site in Brazil. *International Journal of Remote Sensing*, *19*, 3127–3140.

Fuller, D. O. (1999). Canopy phenology of some mopane and miombo woodlands in eastern Zambia. *Global Ecology and Biogeography*, *8*, 199–209.

Fuller, D. O., & Prince, S. D. (1996). Rainfall and foliar dynamics in tropical southern Africa: Potential impacts of global climatic change on savanna vegetation. *Climatic Change*, *33*, 69–96.

Gitelson, A. A., Peng, Y., Masek, J. G., Rundquist, D. C., Verma, S., Suyker, A., et al. (2012). Remote estimation of crop gross primary production with Landsat data. *Remote Sensing of Environment*, *121*, 404–414.

Gitelson, A. A., Vina, A., Verma, S. B., Rundquist, D. C., Arkebauer, T. J., Keydan, G., et al. (2006). Relationship between gross primary production and chlorophyll content in crops: Implications for the synoptic monitoring of vegetation productivity. *Journal of Geophysical Research-Atmospheres*, *111*.

Goerner, A., Reichstein, M., Tomelleri, E., Hanan, N., Rambal, S., Papale, D., et al. (2011). Remote sensing of ecosystem light use efficiency with MODIS-based PRI. *Biogeosciences*, *8*, 189–202.

Higgins, S. I., Delgado-Cartay, M. D., February, E. C., & Combrink, H. J. (2011). Is there a temporal niche separation in the leaf phenology of savanna trees and grasses? *Journal of Biogeography*, *38*, 2165–2175.

Hoffmann, W. A., da Silva, E. R., Machado, G. C., Bucci, S. J., Scholz, F. G., Goldstein, G., et al. (2005). Seasonal leaf dynamics across a tree density gradient in a Brazilian savanna. *Oecologia*, *145*, 307–316.

Huemmrich, K. F., Privette, J. L., Mukelabai, M., Myneni, R. B., & Knyazikhin, Y. (2005). Time-series validation of MODIS land biophysical products in a Kalahari Woodland. Africa. *International Journal of Remote Sensing*, *26*, 4381–4398.

Huete, A., Didan, K., Miura, T., Rodriguez, E. P., Gao, X., & Ferreira, L. G. (2002). Overview of the radiometric and biophysical performance of the MODIS vegetation indices. *Remote Sensing of Environment*, *83*, 195–213.

Huete, A. R., Liu, H. Q., Batchily, K., & vanLeeuwen, W. (1997). A comparison of vegetation indices over a global set of TM images for EOS-MODIS. *Remote Sensing of Environment*, *59*, 440–451.

Hutley, L. B., Beringer, J., Isaac, P. R., Hacker, J. M., & Cernusak, L. A. (2011). A sub-continental scale living laboratory: Spatial patterns of savanna vegetation over a rainfall gradient in northern Australia. *Agricultural and Forest Meteorology*, *151*, 1417–1428.

Hutley, L. B., Leuning, R., Beringer, J., & Cleugh, H. A. (2005). The utility of the eddy covariance techniques as a tool in carbon accounting: Tropical savanna as a case study. *Australian Journal of Botany*, *53*, 663–675.

Hüttich, C., Gessner, U., Herold, M., Strohbach, B. J., Schmidt, M., Keil, M., et al. (2009). On the suitability of MODIS time series netrics to map vegetation types in dry savanna ecosystems: A case study in the Kalahari of NE Namibia. *Remote Sensing*, *1*, 620–643.

Huttich, C., Herold, M., Strohbach, B., & Dech, S. (2011). Integrating in-situ, Landsat, and MODIS data for mapping in Southern African savannas: Experiences of LCCS-based land-cover mapping in the Kalahari in Namibia. *Environmental Monitoring and Assessment*, *176*, 531–547.

John, R., Chen, J., Noormets, A., Xiao, X., Xu, J., Lu, N., et al. (2013). Modelling gross primary production in semi-arid Inner Mongolia using MODIS imagery and eddy covariance data. *International Journal of Remote Sensing*, *34*, 2829–2857.

Jolly, W. M., & Running, S. W. (2004). Effects of precipitation and soil water potential on drought deciduous phenology in the Kalahari. *Global Change Biology*, *10*, 303–308.

Jones, M. O., Kimball, J. S., Jones, L. A., & McDonald, K. C. (2012). Satellite passive microwave detection of North America start of season. *Remote Sensing of Environment*, *123*, 324–333.

Kalfas, J. L., Xiao, X. M., Vanegas, D. X., Verma, S. B., & Suyker, A. E. (2011). Modeling gross primary production of irrigated and rain-fed maize using MODIS imagery and CO_2 flux tower data. *Agricultural and Forest Meteorology*, *151*, 1514–1528.

Kanniah, K. D., Beringer, J., & Hutley, L. B. (2011). Environmental controls on the spatial variability of savanna productivity in the Northern Territory, Australia. *Agricultural and Forest Meteorology*, *151*, 1429–1439.

Kanniah, K. D., Beringer, J., Hutley, L. B., Tapper, N. J., & Zhu, X. (2009). Evaluation of collections 4 and 5 of the MODIS gross primary productivity product and algorithm improvement at a tropical savanna site in northern Australia. *Remote Sensing of Environment*, *113*, 1808–1822.

Kim, Y., Kimball, J. S., Zhang, K., & McDonald, K. C. (2012). Satellite detection of increasing Northern Hemisphere non-frozen seasons from 1979 to 2008: Implications for regional vegetation growth. *Remote Sensing of Environment*, *121*, 472–487.

Kross, A., Fernandes, R., Seaquist, J., & Beaubien, E. (2011). The effect of the temporal resolution of NDVI data on season onset dates and trends across Canadian broadleaf forests. *Remote Sensing of Environment*, *115*, 1564–1575.

Kutsch, W. L., Hanan, N., Scholes, B., McHugh, I., Kubheka, W., Eckhardt, H., et al. (2008). Response of carbon fluxes to water relations in a savanna ecosystem in South Africa. *Biogeosciences*, *5*, 1797–1808.

Kutsch, W. L., Merbold, L., Ziegler, W., Mukelabai, M. M., Muchinda, M., Kolle, O., et al. (2011). The charcoal trap: Miombo forests and the energy needs of people. *Carbon Balance and Management*, *6*, 5.

Larcher, W. (2003). *Physiological plant ecology* (4th ed.). Berlin: Springer.

Li, Z. Q., Yu, G. R., Xiao, X. M., Li, Y. N., Zhao, X. Q., Ren, C. Y., et al. (2007). Modeling gross primary production of alpine ecosystems in the Tibetan Plateau using MODIS images and climate data. *Remote Sensing of Environment*, *107*, 510–519.

Ludwig, F., de Kroon, H., Berendse, F., & Prins, H. H. T. (2004). The influence of savanna trees on nutrient, water and light availability and the understorey vegetation. *Plant Ecology*, *170*, 93–105.

Ma, S. Y., Baldocchi, D. D., Xu, L. K., & Hehn, T. (2007). Inter-annual variability in carbon dioxide exchange of an oak/grass savanna and open grassland in California. *Agricultural and Forest Meteorology*, *147*, 157–171.

McGuire, A. D., Melillo, J. M., Joyce, L. A., Kicklighter, D. W., Grace, A. L., Moore, B., III, et al. (1992). Interactions between carbon and nitrogen dynamics in estimating net primary productivity for potential vegetation in North America. *Global Biogeochemical Cycles*, *6*, 101–124.

Merbold, L., Ardo, J., Arneth, A., Scholes, R. J., Nouvellon, Y., de Grandcourt, A., et al. (2009). Precipitation as driver of carbon fluxes in 11 African ecosystems. *Biogeosciences*, *6*, 1027–1041.

Merbold, L., Ziegler, W., Mukelabai, M. M., & Kutsch, W. L. (2011). Spatial and temporal variation of CO_2 efflux along a disturbance gradient in a miombo woodland in Western Zambia. *Biogeosciences*, *8*, 147–164.

Monteith, J. L. (1972). Solar radiation and productivity in tropical ecosystems. *Journal of Applied Ecology*, 747–766.

Moody, A., & Johnson, D. M. (2001). Land-surface phenologies from AVHRR using the discrete Fourier transform. *Remote Sensing of Environment*, *75*, 305–323.

Oliveira, T., Carvalho, L., Oliveira, L., Lacerda, W., & Acerbi, F., Jr. (2012). NDVI time series for mapping phenological variability of forests across the cerrado biome in Minas Gerais, Brazil. In X. Y. Zhang (Ed.), *Phenology and climate change* (pp. 253–272). Croatia: InTech.

Papale, D., & Valentini, A. (2003). A new assessment of European forests carbon exchanges by eddy fluxes and artificial neural network spatialization. *Global Change Biology*, *9*, 525–535.

Park, S., & Miura, T. (2011). Moderate-resolution imaging spectroradiometer-based vegetation indices and their fidelity in the tropics. *Journal of Applied Remote Sensing*, *5*.
Peng, Y., Gitelson, A. A., Keydan, G., Rundquist, D. C., & Moses, W. (2011). Remote estimation of gross primary production in maize and support for a new paradigm based on total crop chlorophyll content. *Remote Sensing of Environment*, *115*, 978–989.
Pereira, J. S., Mateus, J. A., Aires, L. M., Pita, G., Pio, C., David, J. S., et al. (2007). Net ecosystem carbon exchange in three contrasting Mediterranean ecosystems — The effect of drought. *Biogeosciences*, *4*, 791–802.
Potter, C., Klooster, S., Genovese, V., Hiatt, C., Boriah, S., Kumar, V., et al. (2012). Terrestrial ecosystem carbon fluxes predicted from MODIS satellite data and large-scale disturbance modeling. *International Journal of Geosciences*, *3*, 469–479.
Potter, C. S., Randerson, J. T., Field, C. B., Matson, P. A., Vitousek, P. M., Mooney, H. A., et al. (1993). Terrestrial ecosystem production — A process model-based on global satellite and surface data. *Global Biogeochemical Cycles*, *7*, 811–841.
Prince, S. D., Goetz, S. J., & Goward, S. N. (1995). Monitoring primary production from earth observing satellites. *Water, Air, and Soil Pollution*, *82*, 509–522.
Prince, S. D., & Goward, S. N. (1995). Global primary production: A remote sensing approach. *Journal of Biogeography*, *22*, 815–835.
Raich, J. W., Rastetter, E. B., Melillo, J. M., Kicklighter, D. W., Steudler, P. A., Peterson, B. J., et al. (1991). Potential net primary productivity in South-America — Application of a global-model. *Ecological Applications*, *1*, 399–429.
Reichstein, M., Falge, E., Baldocchi, D., Papale, D., Aubinet, M., Berbigier, P., et al. (2005). On the separation of net ecosystem exchange into assimilation and ecosystem respiration: Review and improved algorithm. *Global Change Biology*, *11*, 1424–1439.
Ruimy, A., Dedieu, G., & Saugier, B. (1996). TURC: A diagnostic model of continental gross primary productivity and net primary productivity. *Global Biogeochemical Cycles*, *10*, 269–285.
Ruimy, A., Saugier, B., & Dedieu, G. (1994). Methodology for the estimation of terrestrial net primary production from remotely sensed data. *Journal of Geophysical Research-Atmospheres*, *99*, 5263–5283.
Running, S. W., Thornton, P. E., Nemani, R., & Glassy, J. M. (2000). Global terrestrial gross and net primary productivity from the earth observing system. In O. E. Sala, R. B. Jackson, H. A. Mooney, & R. W. Howarth (Eds.), *Methods in Ecosystem Science* (pp. 44–57). New York: Springer Verlag.
Sakamoto, T., Gitelson, A. A., Wardlow, B. D., Verma, S. B., & Suyker, A. E. (2011). Estimating daily gross primary production of maize based only on MODIS WDRVI and shortwave radiation data. *Remote Sensing of Environment*, *115*, 3091–3101.
Sakamoto, T., Yokozawa, M., Toritani, H., Shibayama, M., Ishitsuka, N., & Ohno, H. (2005). A crop phenology detection method using time-series MODIS data. *Remote Sensing of Environment*, *96*, 366–374.
Scanlon, T. M., & Albertson, J. D. (2004). Canopy scale measurements of CO_2 and water vapor exchange along a precipitation gradient in southern Africa. *Global Change Biology*, *10*, 329–341.
Scholes, R. J., & Archer, S. R. (1997). Tree-grass interactions in savannas. *Annual Review of Ecology and Systematics*, *28*, 517–544.
Scholes, R. J., & Hall, D. O. (1996). *The carbon budget of tropical savannas, woodlands and grasslands.* New York: John Wiley and Sons.
Scholes, R. J., & Parsons, D. A. B. (1997). *The Kalahari transect: Research on global change and sustainable development in Southern Africa.* (In. Stockholm).
Sims, D. A., Rahman, A. F., Cordova, V. D., El-Masri, B. Z., Baldocchi, D. D., Flanagan, L. B., et al. (2006). On the use of MODIS EVI to assess gross primary productivity of North American ecosystems. *Journal of Geophysical Research-Biogeosciences*, *111*.
Sjöström, M., Ardö, J., Arneth, A., Boulain, N., Cappelaere, B., Eklundh, L., et al. (2011). Exploring the potential of MODIS EVI for modeling gross primary production across African ecosystems. *Remote Sensing of Environment*, *115*, 1081–1089.
Sjöström, M., Ardo, J., Eklundh, L., El-Tahir, B. A., El-Khidir, H. A. M., Hellstrom, M., et al. (2009). Evaluation of satellite based indices for gross primary production estimates in a sparse savanna in the Sudan. *Biogeosciences*, *6*, 129–138.
Sjöström, M., Zhao, M., Archibald, S., Arneth, A., Cappelaere, B., Falk, U., et al. (2013). Evaluation of MODIS gross primary productivity for Africa using eddy covariance data. *Remote Sensing of Environment*, *131*, 275–286.
Skarpe, C. (1992). Dynamics of savanna ecosystems. *Journal of Vegetation Science*, *3*, 293–300.
Tian, Y. H., Woodcock, C. E., Wang, Y. J., Privette, J. L., Shabanov, N. V., Zhou, L. M., et al. (2002). Multiscale analysis and validation of the MODIS LAI product — I. Uncertainty assessment. *Remote Sensing of Environment*, *83*, 414–430.
Tian, Y. H., Zhou, L. M., Romanov, P., Yu, B., & EK, M. (2012). Improving monitoring of tropical forests and their characterizations in NCEP models. *NOAA Satellite Science Week Meeting* (Kansas City, MO).
Townsend, P. A., Singh, A., Foster, J. R., Rehberg, N. J., Kingdon, C. C., Eshleman, K. N., et al. (2012). A general Landsat model to predict canopy defoliation in broadleaf deciduous forests. *Remote Sensing of Environment*, *119*, 255–265.
Tucker, C. J. (1979). Red and photographic infrared linear combinations for monitoring vegetation. *Remote Sensing of Environment*, *8*, 127–150.
Veenendaal, E. M., Kolle, O., & Lloyd, J. (2004). Seasonal variation in energy fluxes and carbon dioxide exchange for a broad-leaved semi-arid savanna (Mopane woodland) in Southern Africa. *Global Change Biology*, *10*, 318–328.
Veenendaal, E. M., Mantlana, K. B., Pammenter, N. W., Weber, P., Huntsman-Mapila, P., & Lloyd, J. (2008). Growth form and seasonal variation in leaf gas exchange of *Colophospermum mopane* savanna trees in northwest Botswana. *Tree Physiology*, *28*, 417–424.
Veroustraete, F., Sabbe, H., Rasse, D. P., & Bertels, L. (2004). Carbon mass fluxes of forests in Belgium determined with low resolution optical sensors. *International Journal of Remote Sensing*, *25*, 769–792.
Vrieling, A., de Beurs, K. M., & Brown, M. E. (2011). Variability of African farming systems from phenological analysis of NDVI time series. *Climatic Change*, *109*, 455–477.
Wagenseil, H., & Samimi, C. (2006). Assessing spatio-temporal variations in plant phenology using Fourier analysis on NDVI time series: Results from a dry savannah environment in Namibia. *International Journal of Remote Sensing*, *27*, 3455–3471.
Wang, H. S., Jia, G. S., Fu, C. B., Feng, J. M., Zhao, T. B., & Ma, Z. G. (2010a). Deriving maximal light use efficiency from coordinated flux measurements and satellite data for regional gross primary production modeling. *Remote Sensing of Environment*, *114*, 2248–2258.
Wang, Z., Xiao, X. M., & Yan, X. D. (2010b). Modeling gross primary production of maize cropland and degraded grassland in northeastern China. *Agricultural and Forest Meteorology*, *150*, 1160–1167.
Weber, U., Jung, M., Reichstein, M., Beer, C., Braakhekke, M. C., Lehsten, V., et al. (2009). The interannual variability of Africa's ecosystem productivity: A multi-model analysis. *Biogeosciences*, *6*, 285–295.
White, M. A., de Beurs, K. M., Didan, K., Inouye, D. W., Richardson, A. D., Jensen, O. P., et al. (2009). Intercomparison, interpretation, and assessment of spring phenology in North America estimated from remote sensing for 1982–2006. *Global Change Biology*, *15*, 2335–2359.
Whitley, R. J., Macinnis-Ng, C. M. O., Hutley, L. B., Beringer, J., Zeppel, M., Williams, M., et al. (2011). Is productivity of mesic savannas light limited or water limited? Results of a simulation study. *Global Change Biology*, *17*, 3130–3149.
Williams, C. A., Hanan, N. P., Neff, J. C., Scholes, R. J., Berry, J. A., Denning, A. S., et al. (2007). Africa and the global carbon cycle. *Carbon Balance and Management*, *2*.
Williams, C. A., Hanan, N., Scholes, R. J., & Kutsch, W. (2009). Complexity in water and carbon dioxide fluxes following rain pulses in an African savanna. *Oecologia*, *161*, 469–480.
Woollen, E., Ryan, C. M., & Williams, M. (2012). Carbon stocks in an African woodland landscape: Spatial distributions and scales of variation. *Ecosystems*, *15*, 804–818.
Wu, C. Y. (2012). Use of a vegetation index model to estimate gross primary production in open grassland. *Journal of Applied Remote Sensing*, *6*.
Wu, C. Y., & Chen, J. M. (2012). The use of precipitation intensity in estimating gross primary production in four northern grasslands. *Journal of Arid Environments*, *82*, 11–18.
Wu, C. Y., Chen, J. M., & Huang, N. (2011). Predicting gross primary production from the enhanced vegetation index and photosynthetically active radiation: Evaluation and calibration. *Remote Sensing of Environment*, *115*, 3424–3435.
Wu, C. Y., Munger, J. W., Niu, Z., & Kuang, D. (2010). Comparison of multiple models for estimating gross primary production using MODIS and eddy covariance data in Harvard Forest. *Remote Sensing of Environment*, *114*, 2925–2939.
Wu, C. Y., & Niu, Z. (2012). Modelling light use efficiency using vegetation index and land surface temperature from MODIS in Harvard Forest. *International Journal of Remote Sensing*, *33*, 2261–2276.
Wu, W. X., Wang, S. Q., Xiao, X. M., Yu, G. R., Fu, Y. L., & Hao, Y. B. (2008). Modeling gross primary production of a temperate grassland ecosystem in Inner Mongolia, China, using MODIS imagery and climate data. *Science in China Series D-Earth Sciences*, *51*, 1501–1512.
Xiao, X. M. (2006). Light absorption by leaf chlorophyll and maximum light use efficiency. *IEEE Transactions on Geoscience and Remote Sensing*, *44*, 1933–1935.
Xiao, X. M., Boles, S., Liu, J. Y., Zhuang, D. F., & Liu, M. L. (2002). Characterization of forest types in Northeastern China, using multi-temporal SPOT-4 VEGETATION sensor data. *Remote Sensing of Environment*, *82*, 335–348.
Xiao, X. M., Hagen, S., Zhang, Q. Y., Keller, M., & Moore, B. (2006). Detecting leaf phenology of seasonally moist tropical forests in South America with multi-temporal MODIS images. *Remote Sensing of Environment*, *103*, 465–473.
Xiao, X. M., Hollinger, D., Aber, J., Goltz, M., Davidson, E. A., Zhang, Q. Y., et al. (2004a). Satellite-based modeling of gross primary production in an evergreen needleleaf forest. *Remote Sensing of Environment*, *89*, 519–534.
Xiao, X. M., Zhang, Q. Y., Braswell, B., Urbanski, S., Boles, S., Wofsy, S., et al. (2004b). Modeling gross primary production of temperate deciduous broadleaf forest using satellite images and climate data. *Remote Sensing of Environment*, *91*, 256–270.
Xiao, X. M., Zhang, Q. Y., Hollinger, D., Aber, J., & Moore, B. (2005a). Modeling gross primary production of an evergreen needleleaf forest using modis and climate data. *Ecological Applications*, *15*, 954–969.
Xiao, X. M., Zhang, Q. Y., Saleska, S., Hutyra, L., De Camargo, P., Wofsy, S., et al. (2005b). Satellite-based modeling of gross primary production in a seasonally moist tropical evergreen forest. *Remote Sensing of Environment*, *94*, 105–122.
Yan, H. M., Fu, Y. L., Xiao, X. M., Huang, H. Q., He, H. L., & Ediger, L. (2009). Modeling gross primary productivity for winter wheat–maize double cropping system using MODIS time series and CO_2 eddy flux tower data. *Agriculture, Ecosystems & Environment*, *129*, 391–400.
Yuan, W. P., Liu, S., Zhou, G. S., Zhou, G. Y., Tieszen, L. L., Baldocchi, D., et al. (2007). Deriving a light use efficiency model from eddy covariance flux data for predicting daily gross primary production across biomes. *Agricultural and Forest Meteorology*, *143*, 189–207.
Zhang, F. M., Chen, J. M., Chen, J. Q., Gough, C. M., Martin, T. A., & Dragoni, D. (2012). Evaluating spatial and temporal patterns of MODIS GPP over the conterminous US against flux measurements and a process model. *Remote Sensing of Environment*, *124*, 717–729.
Zhang, X., Friedl, M. A., & Schaaf, C. B. (2006). Global vegetation phenology from Moderate Resolution Imaging Spectroradiometer (MODIS): Evaluation of global patterns and comparison with in situ measurements. *Journal of Geophysical Research-Biogeosciences*, *111*.
Zhao, M., Running, S. W., & Nemani, R. R. (2006). Sensitivity of Moderate Resolution Imaging Spectroradiometer (MODIS) terrestrial primary production to the accuracy of meteorological reanalyses. *Journal of Geophysical Research-Biogeosciences*, *111*.
Zhu, W. Q., Pan, Y. Z., He, H., Yu, D. Y., & Hu, H. B. (2006). Simulation of maximum light use efficiency for some typical vegetation types in China. *Chinese Science Bulletin*, *51*, 457–463.